Ethan Kung
Mechanical and Aerospace Engineering Department, University of California San Diego, 9500 Gilman Drive MC 0411, La Jolla, CA 92093
e-mail: keo@ucsd.edu

Giancarlo Pennati
Laboratory of Biological Structure Mechanics, Department of Chemistry, Materials and Chemical Engineering "Giulio Natta", Politecnico di Milano, Piazza Leonardo da Vinci, 32, Milan 20133, Italy
e-mail: giancarlo.pennati@polimi.it

Francesco Migliavacca
Laboratory of Biological Structure Mechanics, Department of Chemistry, Materials and Chemical Engineering "Giulio Natta", Politecnico di Milano, Piazza Leonardo da Vinci, 32, Milan 20133, Italy
e-mail: francesco.migliavacca@polimi.it

Tain-Yen Hsia
Cardiorespiratory Unit, Great Ormond Street Hospital for Children, 7th Floor, Nurses Home, London WC1N 3JH, UK
e-mail: hsiat@gosh.nhs.uk

Richard Figliola
Mechanical Engineering Department, Clemson University, 216 South Palmetto Boulevard, Clemson, SC 29634-0921
e-mail: fgliola@clemson.edu

Alison Marsden
Mechanical and Aerospace Engineering Department, University of California San Diego, 9500 Gilman Drive MC 0411, La Jolla, CA 92093
e-mail: amarsden@eng.ucsd.edu

Alessandro Giardini
Cardiorespiratory Unit, Great Ormond Street Hospital for Children, 7th Floor, Nurses Home, London WC1N 3JH, UK
e-mail: alessandro.giardini@gosh.nhs.uk

MOCHA Investigators
Institute of Cardiovascular Sciences, University College London, London W1T 7HA, UK

A Simulation Protocol for Exercise Physiology in Fontan Patients Using a Closed Loop Lumped-Parameter Model

Background: Reduced exercise capacity is nearly universal among Fontan patients, though its etiology is not yet fully understood. While previous computational studies have attempted to model Fontan exercise, they did not fully account for global physiologic mechanisms nor directly compare results against clinical and physiologic data. Methods: In this study, we developed a protocol to simulate Fontan lower-body exercise using a closed-loop lumped-parameter model describing the entire circulation. We analyzed clinical exercise data from a cohort of Fontan patients, incorporated previous clinical findings from literature, quantified a comprehensive list of physiological changes during exercise, translated them into a computational model of the Fontan circulation, and designed a general protocol to model Fontan exercise behavior. Using inputs of patient weight, height, and if available, patient-specific reference heart rate (HR) and oxygen consumption, this protocol enables the derivation of a full set of parameters necessary to model a typical Fontan patient of a given body-size over a range of physiologic exercise levels. Results: In light of previous literature data and clinical knowledge, the model successfully produced realistic trends in physiological parameters with exercise level. Applying this method retrospectively to a set of clinical Fontan exercise data, direct comparison between simulation results and clinical data demonstrated that the model successfully reproduced the average exercise response of a cohort of typical Fontan patients. Conclusion: This work is intended to offer a foundation for future advances in modeling Fontan exercise, highlight the needs in clinical data collection, and provide clinicians with quantitative reference exercise physiologies for Fontan patients. [DOI: 10.1115/1.4027271]

Introduction

Single ventricle physiology is one of the most severe forms of congenital heart disease, in which an infant has only one functional pumping chamber. The condition is not compatible with life without treatment and these infants require immediate surgical

Manuscript received January 4, 2014; final manuscript received March 5, 2014; accepted manuscript posted March 24, 2014; published online June 5, 2014. Assoc. Editor: Tim David.

intervention after birth, typically followed by two additional palliative procedures within the first few years of life. The Fontan procedure, in its various technical modifications, represents the final stage of the multistaged surgery that achieves complete separation of the deoxygenated and oxygenated blood in the circulation. The procedure involves directly connecting the superior venae cavae and inferior venae cavae (SVC and IVC) to the pulmonary arteries, thus bypassing the heart and resulting in the total venous return flowing passively into the pulmonary circulation.

Exercise intolerance is among the myriad complications that contribute to the gradual attrition of post-Fontan patients in the years following surgery. Other causes of decreased survival include ventricular dysfunction, atrial arrhythmias, protein-losing enteropathy, arteriovenous malformations, thrombotic complications, and poor neurodevelopmental outcomes [1]. While most Fontan procedures result in relatively well-performing circulations under resting conditions, the inherent limitations of Fontan physiology often emerge during exercise, causing reduced exercise capacity [2,3]. The etiology of reduced exercise performance is not yet fully understood, and is likely related to multiple causes, including the geometry of the Fontan surgical pathway, the responses of the pulmonary arterial vascular resistances, and the changing loading conditions of the heart [4,5]. Parameters, such as 3D flow velocities, energy dissipation, hepatic flow distribution, pressure, and wall shear stress, have all been studied in conjunction with exercise performance, Fontan outcomes, and normal lung development [6,7].

Exercise conditions place a high demand on the cardiovascular system, often revealing adverse conditions. Patient management plans, including the design of new surgical methods, should account for the behavior of the system under stress. While it would be ideal to collect comprehensive physiologic exercise data in the clinic, many Fontan patients are too young to reliably undergo exercise testing. For those who are able, acquisition of invasive clinical measurements, such as pressure response, during exercise still poses significant challenges and is typically not standard of care. Clinical data in the literature relating to Fontan exercise conditions are therefore scarce. There have only been two studies thus far which reported invasive pressure measurements in exercising Fontan patients [8,9], and the data used in both studies were acquired over three decades ago in the early 1980s. Clinical measurements in routine Fontan exercise testing typically include oxygen consumption and ventilatory ratio, but no pressure and flow parameters. This lack of data motivates the need for modeling methods that can improve understanding of Fontan exercise physiology, and ultimately improve patient management.

Contemporary computational fluid dynamics methods now offer a powerful approach to analyze patient-specific hemodynamic conditions [10,11]. Patient-specific exercise simulations could enable clinicians to stratify the likelihood or severity of exercise intolerance in patients. Simulations also offer a means for virtual testing of the physiologic causes and consequences of a range of exercise dysfunctions. Multiscale modeling, in particular, enables the potential for investigating local hemodynamics in the context of systemic physiological responses. Well-developed physiology models are essential for providing proper reduced-order downstream conditions in multiscale modeling constructs.

Despite the need for increased understanding of Fontan exercise response, prior modeling efforts to describe Fontan physiology have mainly focused on the effects of varying Fontan connection geometries, and typically have not incorporated the dynamic physiologic response or considered the full range of hemodynamic conditions that can occur within the patient population [12]. Due to the lack of a comprehensive set of clinical data describing exercise conditions, the few prior studies that have attempted to simulate exercise conditions [3,5,13,14] have primarily adopted open-loop models, requiring numerous assumptions for increasing flow rates, changing waveform shapes, and prescribing changes in pulmonary vascular resistances (PVR). Such approaches not only result in pressure and flow predictions that have inherently large uncertainty, but also restrict the investigation to local 3D hemodynamics in isolation from the physiologic response. In addition, there have been essentially no direct comparisons of prior exercise simulations against clinical data. As a result, there is a need for modeling approaches that incorporate systemic physiology and systematic model-parameter selection, increased clinical data collection in Fontan patients during exercise, and validation of Fontan exercise modeling results against clinical data.

In this study, we take an initial step toward addressing the aforementioned deficiencies by developing a protocol based on clinical and literature data to perform simulations of Fontan lower-body exercise using a closed-loop lumped-parameter network (LPN). Using inputs of patient weight, height, and if available, a patient-specific reference HR and oxygen consumption, this protocol enables the derivation of a full set of parameters necessary to model a typical Fontan patient over a range of body-size and physiologic exercise levels. Literature data were combined with a training set of clinical data containing measurements from nine Fontan patients to provide the supporting bases for the protocol development. A separate set of clinical data containing measurements from eight additional Fontan patients was held back to enable direct comparisons between simulation results and clinical data of Fontan exercise.

Methods

We constructed an LPN using a circuit analogy to model the Fontan circulation based on previous works [15–17] (Fig. 1). Similar LPN models were used in previous multiscale simulations which investigated surgical variations of stages 1 and 2 Fontan procedures [10,16,18]. The LPN features modular blocks to mimic major parts of the circulation, with each block responding to pressure and flow according to its physiological counter-part. Appendix A details the implementation of the Fontan LPN framework we constructed for the development of the exercise modeling protocol in this study. To prescribe exercise conditions in the model, one must define a protocol to systematically adjust all LPN parameters based on exercise intensity. This involves determination of systemic and pulmonary resistance, heart function, HR, and other parameters. Below, we describe in detail how these parameters are determined based on available clinical and physiologic data. The individual parameters then interact together in the closed-loop LPN model to produce a holistic systemic physiology of a virtual Fontan patient.

Exercise and Body-Size Dependent Parameters. In this section, we describe the protocol used to define parameter values according to exercise level and patient body-size. Exercise level is expressed in terms of metabolic equivalent (MET), where 1 MET is defined as an oxygen consumption of $3.5\,\text{ml-O}_2\,\text{kg}^{-1}\,\text{min}^{-1}$. Inputs of patient height in centimeters, and weight in kilograms, return the body surface area (BSA) in square meters via the commonly used clinical equation

$$\text{BSA} = \frac{\sqrt{\text{Height} * \text{Weight}}}{3600} \tag{1}$$

From clinical data collected in 17 Fontan patients who underwent exercise testing via the same protocol as our previous study [19], nine Fontan patients (median age 26 years (range 17–30), 1 male) with a resting cardiac index between 1.5 and $4\,\text{l}\,\text{min}^{-1}\,\text{m}^{-2}$ (indicating a clinically normal physiology without severe heart failure) were randomly selected. The patients exercised at different workloads on an upright ergometry bicycle (Table 1). Cardiac output (CO) was measured via pulmonary blood flow using a well-established foreign gas rebreathing technique (Innocor Device, Innovision, Odense, Denmark) [20,21]. Additional details of the clinical data acquisition methods are described in our previous publication [19]. All data were collected in accordance with

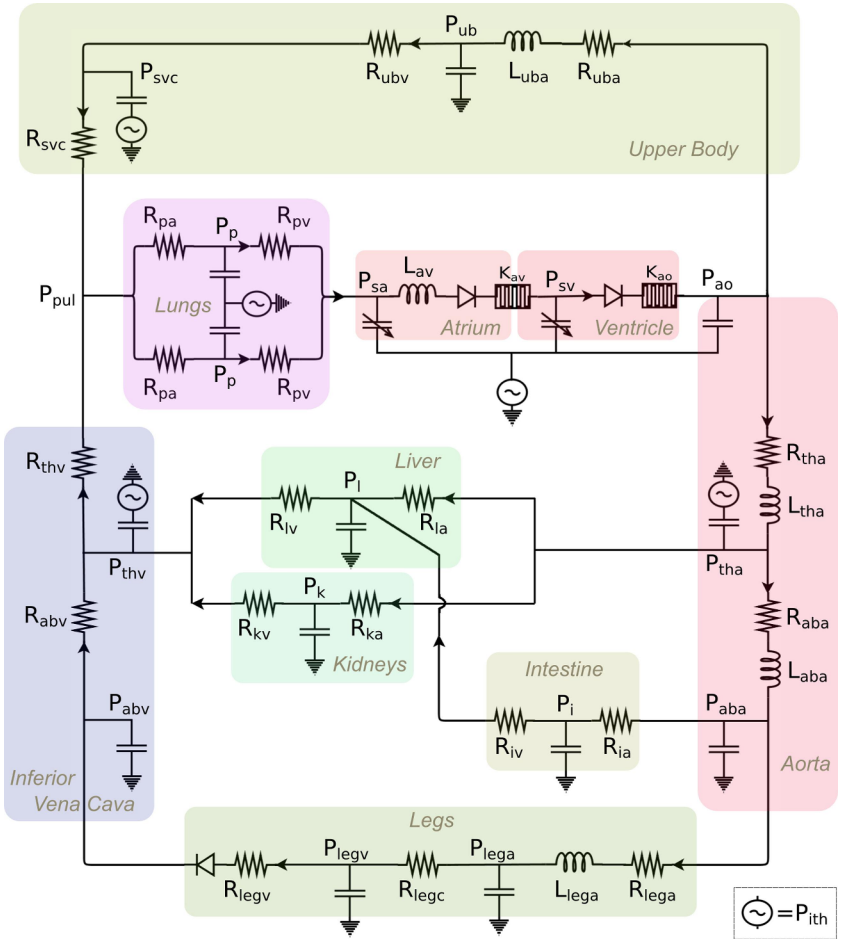

Fig. 1 Closed-loop lumped-parameter network of the Fontan circulation. $R_{subscript}$, $L_{subscript}$, and $P_{subscript}$ are labels for resistor components, inductor components, and nodal pressures, respectively.

Table 1 Clinical characteristics of Fontan patients in study

	Model construction ($n=9$)	Model validation ($n=8$)
Age at test (years)	26 (17–30)	26 (16–31)
BSA (m^2)	1.5 ± 0.2	1.6 ± 0.2
Female gender (n)	8	5
Type of cardiac defect (n)		
Tricuspid atresia	8	5
Double inlet left ventricle	1	3
Type of Fontan operation (n)		
Atriopulmonary	2	2
Extracardiac total cavopulmonary connection	7	6
Peak workload (W)	67 ± 17	72 ± 21
Peak HR	137 ± 17	115 ± 32
V_{O2} at peak CO (ml kg^{-1} min^{-1})	18 ± 3.4	22 ± 4.7
Peak cardiac index (l min^{-1} m^{-2})	4.7 ± 0.7	4.8 ± 1.0

institutional review board guidelines. From this clinical data, we established correlations between exercise levels and HR and total vascular resistance (TVR) (Fig. 2). The TVR was calculated using the measured aortic pressure and CO, with an assumption of 8 mm Hg mean atrial pressure. HR was normalized to weight in accordance with previously published allometric scaling data [22]. Vascular resistance, which is a linear function of blood pressure and flow, was normalized to BSA since blood pressure is known to be invariant with respect to body-size and CO has been shown to scale with BSA [23]. We identified mathematical fits to the clinical data based on the criteria of maximizing correlation coefficients and producing simple functions that resemble the clinical data distribution. These clinical correlations produced the following relationships:

$$\mathrm{HR} = \frac{1}{\mathrm{Weight}^{0.25}}\left(212.4\ \mathrm{MET}^{0.3016}\right) \tag{2}$$

$$\mathrm{TVR} = \frac{1}{\mathrm{BSA}}\left(-8.882\ln(\mathrm{MET}) + 33.00\right) \tag{3}$$

Using the same clinical data, we also provide the correlation ($R^2 = 0.87$) between exercise levels expressed in terms of MET versus power to weight ratio in W/kg to enable translation between the two common measures of exercise level, allowing other investigators to utilize the methods presented in this study in wider ranges of scenarios

$$\mathrm{MET} = 3\mathrm{PWR} + 1 \tag{4}$$

Correlations between exercise level and cardiac index as well as O_2 extraction are also derived directly from the training clinical dataset (Appendix B). This information is not used as part of the simulation protocol described in this study, but is provided here for completeness.

The PVR in Fontan patients' affects the pressure measured in the Fontan pathway, and is speculated to be an important factor limiting exercise tolerance [9,24]. Pulmonary pressure

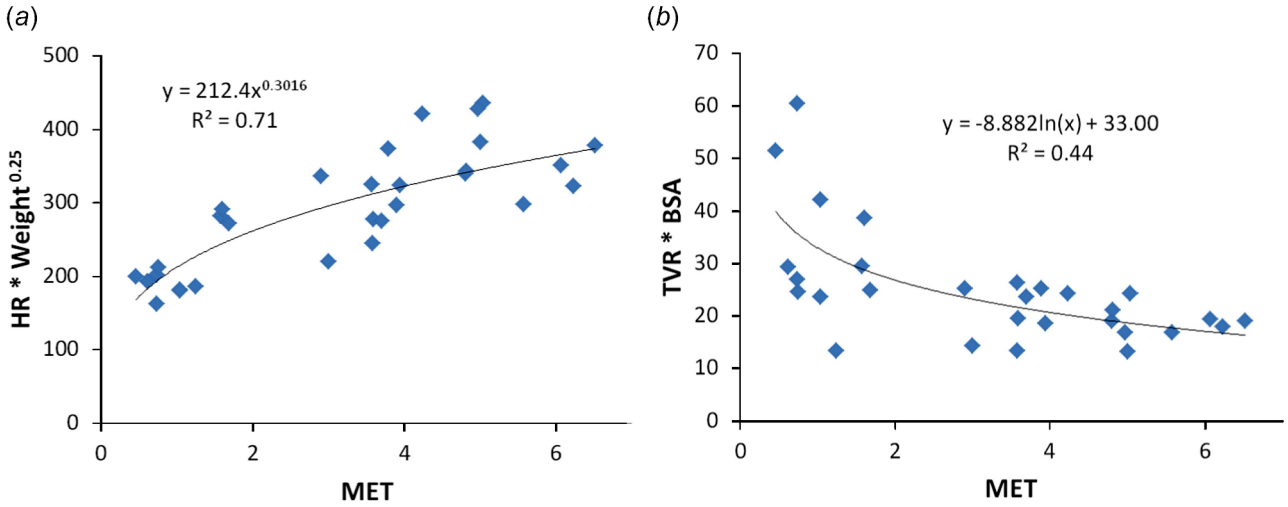

Fig. 2 Exercise clinical data from nine Fontan patients. Plots show correlations of (*a*) normalized HR, and (*b*) normalized TVR, to exercise level expressed in MET.

measurements require invasive catheterization procedures with ethical limitations and are difficult to acquire during exercise, thus literature data relating PVR changes to exercise level are scarce. To establish a reasonable estimate of the relationship between PVR change and exercise, invasive pressure data for at least two levels of exercise are required. An extensive literature search identified only one prior study providing invasive pressure data during graded exercise in patients that could contribute to the construction of this protocol. Via a radial arterial catheter and a Swan-Ganz catheter, Stickland et al. acquired systemic arterial pressure, pulmonary arterial pressure, and pulmonary artery wedge pressure in human subjects at rest and two levels of exercise [25]. Based on this data, we defined a relationship between the change in TVR (relative to resting condition) due to exercise and the corresponding change in PVR

$$\mathrm{PVRf} = 0.4329\ln(\mathrm{TVRf}) + 1 \tag{5}$$

where PVRf and TVRf are the factors that scale the resting values of PVR and TVR, respectively, to their corresponding exercise values.

Even though the data from Stickland et al. were obtained only in healthy adults, Eq. (5) agrees well with clinical measurements made in another study by Shachar et al., who calculated PVR and systemic vascular resistance (SVR) in control and Fontan children at rest and one level of exercise via catheter pressure measurements and Fick principle CO measurements [8]. In control subjects, where the average exercise TVR was 65% that of resting, Eq. (5) predicts a PVR scaling of 82%, and the reported PVR scaling was 80%. In Fontan subjects, where the average exercise TVR was 54% that of resting, Eq. (5) predicts a PVR scaling of 74%, and the reported PVR scaling was 65%.

The systolic time interval (t_{svs}) is one of the parameters used to un-normalize the elastance function described in Appendix A. The systolic fraction is typically one-third of the cardiac cycle at rest, and can increase to about one half of the cardiac cycle at exercise. Previous studies have measured systolic/diastolic time ratios in humans and correlated them to HR [26,27]. We implemented the t_{svs} calculation based on measurements reported by Gemignani et al. which showed a linear increase in systolic/diastolic time ratio with HR up to 120 bpm [27]

$$t_{\mathrm{svs}} = \begin{cases} \left[0.5 - \dfrac{0.2}{60}(120 - \mathrm{HR})\right] * \left(\dfrac{60}{\mathrm{HR}}\right), & \mathrm{HR} \le 120 \\ 0.5 * \left(\dfrac{60}{\mathrm{HR}}\right), & \mathrm{HR} > 120 \end{cases} \tag{6}$$

The $E_{\max}$ parameter is a measure of contractility, which is known to increase with exercise [28]. Considering the reported measurements of $E_{\max}$ made by Alpert et al. in healthy children at rest and two levels of exercise [29] (which had similar values as those reported by Bombardini et al. [30]), and tuning to the actual CO measurements in our training clinical data made in Fontan patients, we defined the following equation to describe the value of $E_{\max}$ at different levels of exercise for different body-sizes:

$$E_{\max} = \mathrm{BSA}(0.326\ \mathrm{MET} + 1.32) \tag{7}$$

As exercise level increases, the diastolic time shortens due to reduced cardiac cycle length as well as diastolic/systolic ratio, while the stroke volume (SV) increases. This implies an increased ventricular filling over a shorter time, meaning there thus must be an increased atrial and ventricular pressure difference during diastole to facilitate the higher ventricular filling rate. Studies have reported mixed findings regarding whether this pressure difference increase occurs through elevated atrial pressure, or decreased ventricular pressure. Investigators have found increased, decreased, and unchanged atrial pressures with exercise in humans [31–35]. Some have found an initial increase and then a subsequent decrease in atrial pressure during exercise [36–40]. In animals, investigators have also found both significantly elevated atrial pressures [41,42], and constant atrial pressure with decreased ventricular diastolic-onset pressure [43] during exercise. The E_{offset} parameter described in Appendix A dominates the ventricular pressure–volume relationship during diastole, and thus has the largest effect on ventricular filling. Tuning to achieve proper filling of the ventricle, reasonable diastolic pressure–volume relationships, and matching CO relative to our training clinical data at various exercise levels, we defined this parameter using the following equation:

$$E_{\mathrm{offset}} = -0.016\ \mathrm{MET} + 0.215 \tag{8}$$

The ventricular reference volume (V_{svo}) is a parameter affecting the horizontal location of the ventricular pressure–volume loop. Based on literature data of end diastolic and systolic volume (EDV and ESV) measurements in humans [30,44,45], and clinical knowledge of ejection fractions (EF) that represent typical Fontan patients, we define an equation for V_{svo} that results in realistic pressure–volume loops

$$V_{\mathrm{svo}} = 67\ \mathrm{BSA} - 100 \tag{9}$$

Table 2 Reference lumped-parameter network parameter values. Capacitances are labeled with subscripts corresponding to the most immediately adjacent nodal pressures in Fig. 1.

Resistance (mm Hg s ml^{-1})	
R_{uba}	0.573
R_{ubv}	2.000
R_{tha}	0.068
R_{aba}	0.517
R_{lega}	1.269
R_{legc}	3.000
R_{legv}	0.699
R_{abv}	0.050
R_{thv}	0.025
R_{la}	7.154
R_{lv}	0.045
R_{ka}	5.039
R_{kv}	0.472
R_{ia}	11.048
R_{iv}	0.201
R_{pa}	0.020
R_{pv}	0.100
R_{svc}	0.050
Capacitance (ml mm Hg^{-1})	
C_{svc}	2.00
C_{ub}	4.30
C_{ao}	0.70
C_{tha}	0.21
C_{aba}	0.44
C_{lega}	1.96
C_{legv}	10.00
C_{abv}	9.00
C_{thv}	1.00
C_{l}	6.05
C_{k}	2.52
C_{i}	1.51
C_{p}	2.00
Initial Pressure (mm Hg)	
C_{svc}	13.2
C_{ub}	79.4
C_{ao}	94.4
C_{tha}	92.6
C_{aba}	92.6
C_{lega}	66.2
C_{legv}	22.1
C_{abv}	13.2
C_{thv}	13.2
C_{l}	9.7
C_{k}	17.6
C_{i}	9.7
C_{p}	7.9
Initial volume (ml)	
V_{sa}	12.2
V_{sv}	105.4

Using measurements reported by Grimby et al. of intrathoracic pressure in adult humans at rest and two levels of exercise [46], we derived equations to describe the amplitude and offset of the thoracic pressure (AP_{ith} and $P_{ithoffset}$) at different exercise levels

$$AP_{ith} = -3.9 \text{ MET} \tag{10}$$

$$P_{ithoffset} = 1.92(\text{ MET} - 1) - 3.7 \tag{11}$$

These parameters are used to define the thoracic pressure waveform described in Appendix A.

Work-Flow for Derivation of LPN Parameter Values. This section describes the work-flow for deriving a full set of LPN parameters to model a specific patient at a particular exercise level. Tuned based on previous LPN modeling work [16,18], Table 2 lists a set of generic reference values serving as the starting point for the LPN parameters. This generic reference provides the distributed resistance and capacitance values, and initial pressures in the capacitors, to be scaled. Using Table 2 together with Eqs. (1)–(14), we derive the parameters needed to fully define a patient-specific simulation of Fontan exercise.

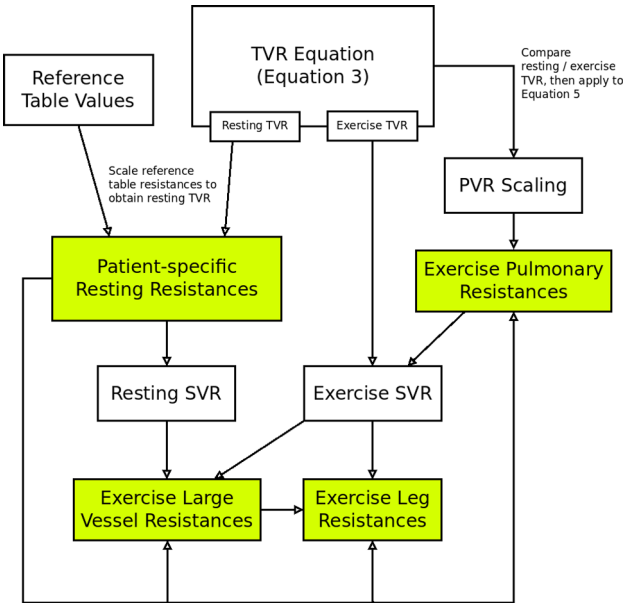

Fig. 3 Flow diagram for computing resistance values in the LPN. Highlighted items represent lists of resistance values used to construct the final list of resistance values in the LPN for a simulation.

Figure 3 shows a flow diagram of the process to appropriately define the resistance values in the LPN. Entering the BSA and MET levels into Eq. (3) enables calculation of the patient-specific resting and exercise TVR. A network analysis of the LPN with the generic reference resistances in Table 2 returns the generic TVR, which is then compared with the patient-specific resting TVR (calculated from Eq. (3)) to return a TVR scaling factor. The *patient-specific resting resistances* are then calculated by scaling the generic resistances by the TVR scaling factor. In addition, using the resting and exercise TVR found from Eq. (3), Eq. (5) returns the PVR scaling factor at exercise. We then scale the pulmonary resistances in the *patient-specific resting resistances* according to this scaling factor and obtain the *exercise pulmonary resistances*.

The exercise SVR is found from the *exercise pulmonary resistances* together with the exercise TVR derived from Eq. (3) (Note that TVR = SVR + PVR). The resting SVR is found via a network analysis of the *patient-specific resting resistances*. The changes in the systemic resistances from resting to exercise are not uniform across the body, as the cardiovascular system adapts to exercise by increasing flow specifically to the active muscles, with little to no increase in blood flow to other parts of the circulation [47]. The effect of the muscle pump is incorporated as an "effective resistance" of the relevant circuits, which is greatly reduced from its resting values. To modify the systemic resistances in our computational model for the exercise condition, we start from the *patient-specific resting resistances*, and first scale the resistances in the aorta blocks (R_{thao}, R_{abao}) according to the ratio of exercise to resting SVR; we then iteratively scale the leg resistances and evaluate the SVR via an LPN network analysis, until the desired exercise SVR is achieved.

In the case of growth, vascular resistance and capacitance scale with body-size via an exponential coefficient of −3 and 4,

Table 3 Mean values of output parameters from simulations of two example patients at various exercise levels. Refer to glossary and Fig. 1 for parameter labels. Q_{svc} and Q_{ivc} are in units of l/min.

(a) Example patient A: weight = 50 kg and height = 150 cm

MET	HR	CO	SV	EF	P_{ao}	P_{sa}	P_{pul}	Q_{svc}	Q_{ivc}	O_2 extraction
1	80	3.54	45.0	0.523	89.7	8.0	12.3	1.48	2.07	0.049
2	98	4.64	47.1	0.574	94.3	7.8	12.8	1.56	3.08	0.076
3	111	5.40	48.5	0.620	95.7	8.5	14.0	1.56	3.84	0.097
4	121	6.08	50.0	0.661	96.6	9.4	15.2	1.56	4.51	0.115
5	130	6.98	55.6	0.704	100.0	9.3	15.6	1.62	5.38	0.125
6	137	7.91	57.8	0.733	103.0	9.3	16.1	1.66	6.24	0.133

(b) Example patient B: weight = 75 kg and height = 180 cm

MET	HR	CO	SV	EF	P_{ao}	P_{sa}	P_{pul}	Q_{svc}	Q_{ivc}	O_2 extraction
1	72	4.68	65.2	0.514	87.8	7.4	11.6	1.95	2.73	0.056
2	89	6.22	69.9	0.548	93.3	6.8	11.9	2.09	4.13	0.084
3	101	7.31	72.6	0.575	95.1	7.3	12.8	2.11	5.19	0.108
4	110	8.10	74.5	0.596	95.2	8.2	14.0	2.09	6.03	0.130
5	117	8.78	75.4	0.615	94.6	9.5	15.4	2.04	6.74	0.149
6	124	9.62	77.8	0.629	95.5	10.2	16.3	2.04	7.61	0.164

respectively. Thus according to the TVR scaling, we scale all of the capacitances to adjust for body-size using the equation [16,18,48]

$$\frac{C}{C_i} = \left(\frac{\text{TVR}}{\text{TVR}_i}\right)^{\frac{-4}{3}} \tag{12}$$

where C/C_i and TVR/TVR_i are the capacitance and TVR scaling ratios, respectively. Terms with subscript "i" indicate the parameter prior to scaling.

In vasodilation or vasoconstriction, vascular resistance and capacitance scale to reflect changes in vessel diameters via an exponential coefficient of −4 and 3, respectively. Thus according to the resulting scaling of resistances due to exercise, we further scale capacitances in the corresponding blocks using the equation [16,18,48]

$$\frac{C}{C_i} = \left(\frac{R}{R_i}\right)^{\frac{-3}{4}} \tag{13}$$

where C/C_i and R/R_i are the capacitance and resistance scaling ratios, respectively. The capacitances in the leg circuit are not scaled since the exercise "effective resistances" largely represent the consequences of the muscle pump, rather than vasodilation alone.

It is well known that the HR of an individual can be affected by fitness level. However, Clausen et al. found that training does not affect the slope of HR increase with exercise [49]. In other words, at a higher fitness level, the reduction in HR during exercise is the same as the reduction in HR at rest. At any particular level of exercise, the increase in HR in excess of the resting value is thus the same regardless of training. We use this finding to incorporate the patient fitness level in the computational model via an offset in HR, if a clinically measured reference HR and MET level for the patient is available. Using the HR calculated from Eq. (2) at the reference MET level, and comparing it with the actual measured reference HR, we obtain the HR offset for the particular patient. We then apply the same HR offset for computations at other MET levels of the same patient.

Lastly, based on the aortic pressure measurements in the training set clinical data, and tuning to the CO measurements, we derive an equation to scale the initial pressures and volumes in Table 2 by the scaling factor "S_{init}" according to exercise level

$$S_{\text{init}} = 0.058\ \text{MET} + 0.942 \tag{14}$$

The remaining parameters of the LPN model are set according to Eqs. (6)–(11).

Results

We applied the protocol described in the Methods section to simulate exercise in a cohort of example and patient-specific models at various MET levels. All cases were simulated for 12 s using 20 microsecond time steps. The last four cardiac cycles (one breathing cycle) of data, after stable periodicity was established, were used for analysis.

Simulated Exercise Physiology of Two Example Patients. Table 3 shows the averaged values of different output parameters from simulations of two example patients at six different MET levels. We simulated a smaller patient with weight = 50 kg and height = 150 cm, and a larger patient with weight = 75 kg and height = 180 cm, to demonstrate the simulation results from the modeling protocol over a range of body-sizes. Physiologically realistic values were obtained for all output parameters in both the smaller and larger body-size example patients. The larger example patient exhibited higher SV and CO as expected. In both example patients, the HR, CO, SV, EF, and O_2 extraction increased steadily with exercise as expected. The increase in CO is mediated via increased IVC flow, with the SVC flow staying relatively constant. The values and trends of EF are consistent with previous literature reports [30,44,45]. The resulting atrial pressures are similar to values reported by Leupker et al., and remain relatively steady at different MET levels with some increases at high MET levels as clinically observed during continuous exercise [36]. However, it is to be noted that a transient increase in atrial pressure at the onset of exercise [36], and a marked increase in atrial pressure during exercise [8], have also both been observed clinically.

The pulmonary pressures predicted in the two example patients are similar to those reported by Shachar et al., who measured right atrial pressure and pulmonary conduit pressure gradient in tricuspid atresia patients with lateral tunnel Fontan palliation during resting and exercise conditions [8]. An increase in up to 30%–40% (4–5 mm Hg) in pulmonary pressure between MET levels was observed in the simulation results, where the data reported

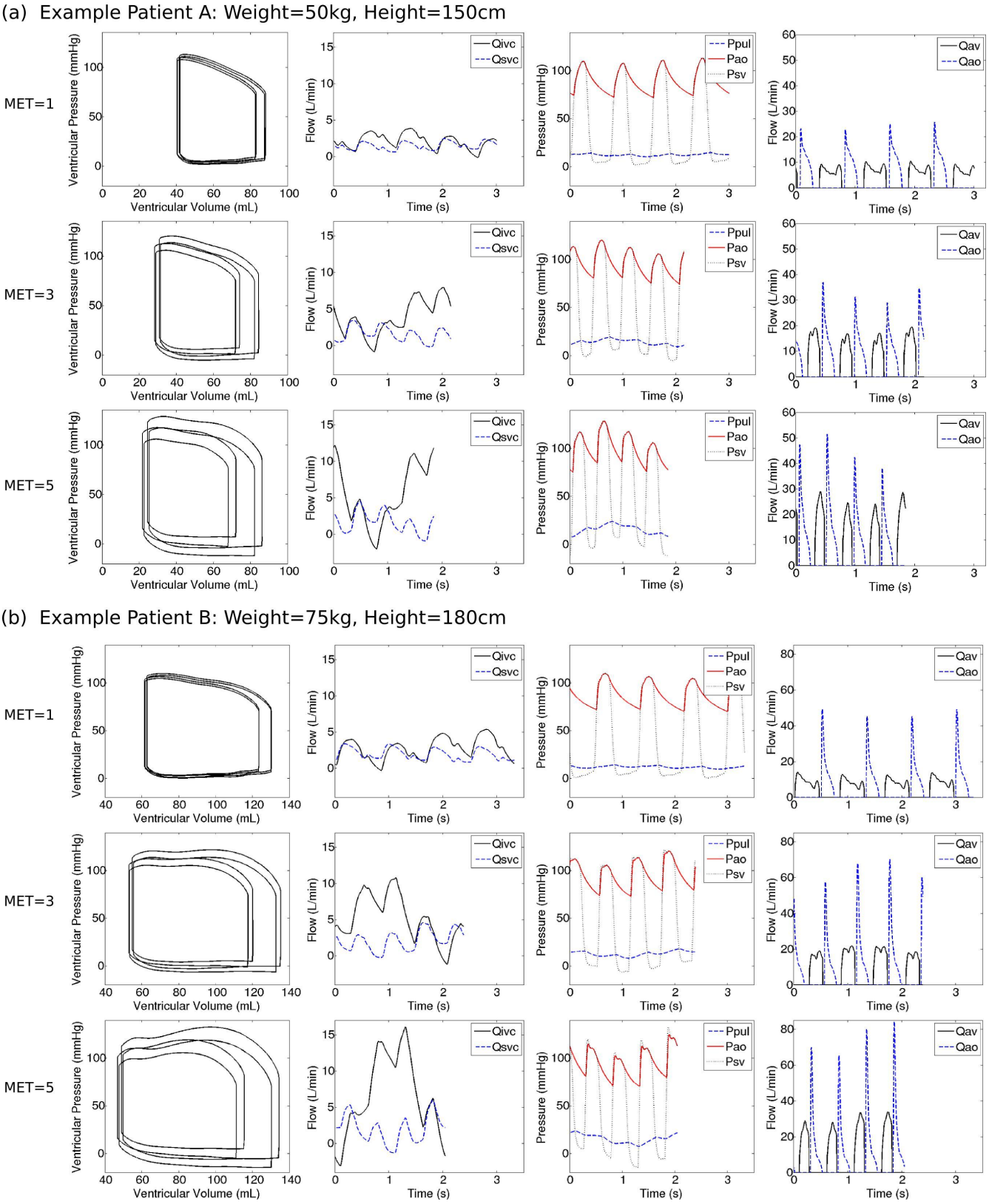

Fig. 4 Simulation results of two example patients at various exercise levels

by Sharchar et al. indicated an increase in approximately 30% (~4 mm Hg) pulmonary pressure from rest to exercise.

From the same simulations of the two example patients, we extract time-dependent details of various output parameters (Fig. 4). The ventricular pressure–volume loops show increased ventricular volume for the larger example patient, and increased SV with exercise as expected. The increase in SV is mediated mainly via a decreased ESV, rather than an increased EDV. The ventricular diastolic pressure decreases with exercise and even becomes negative as respiration (thoracic pressure amplitude) increases. Similar ventricular filling characteristics have been observed in-vivo [43,45]. The effects of breathing on the

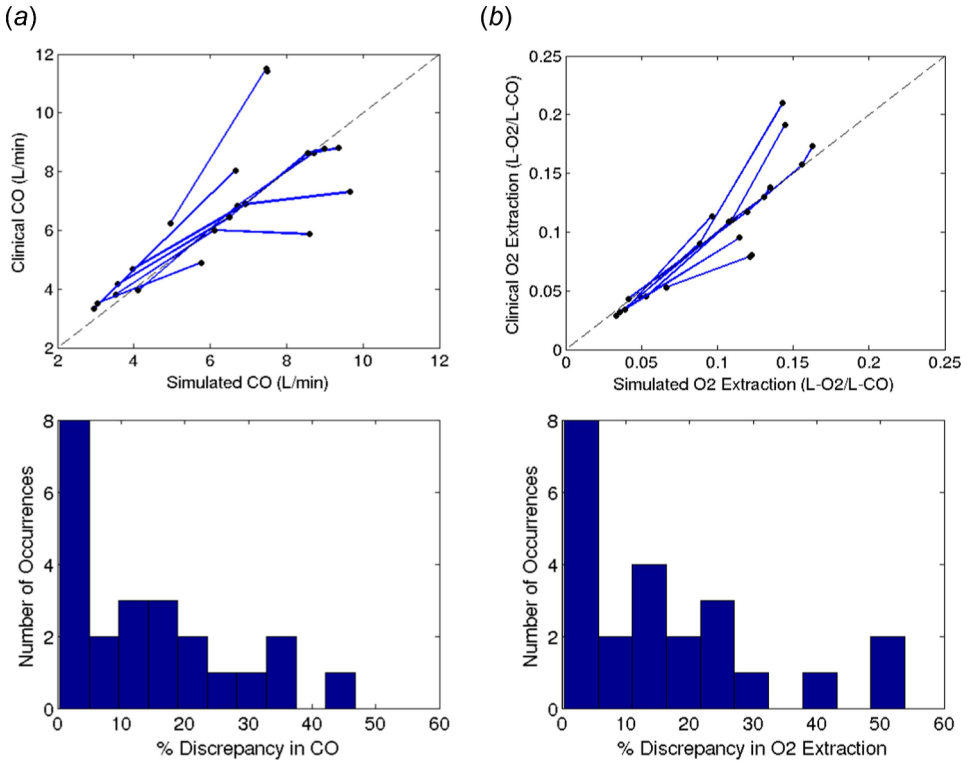

Fig. 5 Model validation of (*a*) CO and (*b*) O_2 extraction against clinical data. Points connected by lines are results of the same patient at different exercise levels.

pressure–volume loop become significantly more pronounced at increasing levels of exercise, manifesting as increased cardiac cycle-to-cycle variations across the breathing cycle.

The SVC flow in both example patients is relatively unaffected by exercise, where the IVC flow increases significantly and clearly exhibits increased respiratory effects with increasing exercise level. Retrograde flow of up to 3% (patient A) and 4% (patient B) occurs in the IVC during exercise. Hjortdal et al. reported clinically measured IVC retrograde flow of ∼3% during exercise (∼10% at rest) [50]. Aortic pressure tracings are realistic, showing physiologic values of systolic and diastolic pressure, for both example patients at all simulated MET levels. The pressure waveforms in the heart, aorta, and pulmonary artery all exhibit increasing influence of respiration across the breathing cycle at higher levels of exercise.

The ventricular filling waveform (Q_{av}) shows a biphasic shape at rest which transitions into a monophasic shape at exercise as the two peaks gradually merge. This phenomenon is consistent with the clinical observations made by Carroll et al. [45]

Comparison Against Clinical Data. A second group of eight different Fontan patients (median age 26 years (range 16–31), 3 male) from our clinical dataset was used for preliminary model validation (Table 1). Figure 5 shows the comparison of CO and O_2 extraction between clinical measurement and simulation prediction, and histograms of the corresponding percent discrepancies. Relative to the clinical measurements, the average discrepancies in simulated results of CO and O_2 extraction were 14.4% and 16.4%, respectively. A direct prediction of CO and O_2 extraction using the equations in Appendix B returned 14.3% and 15.7% average discrepancies against clinical measurements, respectively. Histograms in Fig. 5 show that while most simulated results exhibit less than 30% discrepancy compared with clinical measurements, larger discrepancies do occur in a few cases.

Model Sensitivity Analysis. We performed a comprehensive sensitivity analysis on the LPN model around operating points which describe an example patient with a body weight of 50 kg and height of 150 cm at different MET levels. We found that as exercise level changes, the order of sensitivity toward different input parameters changes as well. At resting condition, the model is most sensitive to the parameters S_{init}, E_{offset}, and E_{max}, where a 10% increase in each resulted in a 8.1%, −4.1%, and 3.1% change in CO, respectively. At five MET, the model becomes most sensitive to the parameters t_{svs}, S_{init}, and TVR, where a 10% increase in each resulted in a −11.1%, 7.9%, and −4% change in CO, respectively. We note that a HR increase results in a decrease in SV, and thus does not result in a directly proportional increase in the CO. Lastly, for all of the input and output parameters examined, we found approximately linear sensitivity relationships when an input parameter is scaled by a small amount (<10%) around its reference point.

Discussion

This work reviews all of the recent relevant physiologic and clinical data related to Fontan exercise and compiles them together into the context of one single computational model, which has not been done previously. A thorough literature review provides a summary of what is known and unknown, and directions for future modeling efforts and clinical data acquisition. The study then takes a reductionist approach and uses the available sources of literature and clinical data to define changes in individual components in the LPN for different exercise levels. Through complex interactions, these parameter changes then produce a coherent holistic systemic response in a closed-loop LPN structure. The model successfully reproduced expected trends in output parameter changes with exercise level. In addition, clinically expected body-size scaling effects were observed in the model outputs, where the blood flow, HR, and blood pressure scaled positively, negatively, and nully, with body-size, respectively. The serendipitous agreement between clinically observed and simulated atrioventricular flow waveform shape change from rest (double peak) to exercise (single peak) provides additional confidence that the

proposed exercise modeling protocol produces realistic physiological behaviors.

The values of the output parameters from the simulations are shown to be similar to general clinical findings from previous literature. Physiologically realistic values were obtained for all relevant output parameters, indicating that the model produces reasonable approximations of physiological behaviors across the circulation over a range of exercise conditions.

Comparison of the CO and O_2 extraction results against a small set of clinical data (that was not used in the original model construction) served as an initial validation of the modeling methods, with discrepancies within reasonable clinical tolerances. It is important to note that CO and O_2 extraction predictions are not, in and of themselves, the primary motivators of our model development, since the model predictions perform roughly equally to those directly obtained using Appendix B equations. Our primary motivation for future applications of this model is to provide a test-bed for investigating hypotheses of exercise dysfunctions and physiologic causes of Fontan exercise intolerance, providing missing insights where clinical data collection is challenging. The model simultaneously reveals interactions between circulatory parameters and underlying physiological mechanisms, which provides more utility than "black box" parameter predictions derived simply from population fits. For the investigation of Fontan exercise physiology, and development of other advanced computational or in-vitro models, the proposed framework provides a basis for incorporating future clinical data, and obtaining insight into possible mechanisms of exercise dysfunction. For example, the detailed time tracings of ventricular pressure–volume loop, aortic pressure, and flows through the aortic and atrioventricular valves provided by this model can be used to design physical experiments, or boundary conditions in multiscale computations, in the investigation of heart valve insufficiencies under various realistic exercise conditions. The model can also be used as a standalone tool to investigate the detailed interactions of different physiological parameters in a closed-loop Fontan circulation model during resting and exercise.

Pulmonary pressure (P_{pul}) has been considered a significant indicator for predicting Fontan outcome and performance. Accurate clinical measurements of this parameter require invasive catheterization procedures and are difficult to perform during exercise. Without prescribing comprehensive parameter changes according to exercise level, it is impossible for a model to predict P_{pul}. Modeling efforts which employed manually imposed flow rates/pulmonary resistance changes have produced exercise Fontan pulmonary pressures that were questionably high [13,51,52], while some have produced results that happened to be similar to those in this study [53]. In studies that have reported exercise P_{pul} results that were drastically higher than those reported in this study, Koeken et al. employed a manually enforced two fold increase in pulmonary flow and fixed pulmonary resistance in an open-loop model [52], and Marsden et al. employed manually enforced 2–3 fold increases in IVC flow together with 5–15% decreases in pulmonary resistance from resting [13,51]. The correlations between the manually enforced flow increases and pulmonary resistance decreases during exercise in these previous studies were based on limited clinical data, resulting in drastic variations in P_{pul} predictions via open-loop systems. In the present model, P_{pul} predictions are arrived at through literature-derived PVR changes interacting with output parameters of the model, such as P_{sa} and CO, leading to results that are instead based on concrete data and closed-loop model interactions. While further validation is still needed, the ability of the model to output P_{pul} provides a useful basis for future investigations into changes in P_{pul} with exercise. However, while the simulated results of P_{pul} agree well with previously measured average P_{pul} in a population of Fontan patients [8], higher exercise P_{pul} values have also been reported [9]. More comprehensive patient-specific clinical data of pulmonary pressures during exercise are required to thoroughly validate P_{pul} predictions to gain further confidence in the model.

Limitations. Before any computational tool is to be utilized, it is important to understand its limitations. Here, we lay out the limitations of the protocol presented in this study. The protocol allows inputs of patient size (weight and height) and a desired exercise level, and returns an estimate of multiple parameters in the systemic physiology. While many output parameters we examined exhibited realistic physiologic behaviors, the only parameters that were directly compared against patient-specific clinical data were the CO and O_2 extraction. Due to the lack of existing clinical measurements, other parameters, such as the flow and pressure waveforms in the various abdominal organs, have not been fully confirmed and should be used with reservation.

The comparison of simulated CO against clinical data shows that although the model prediction average discrepancy is only approximately 14%, there can be outlier patients with larger differences between the predictions and clinical measurements. The model is designed to be "patient-specific" to the extent allowed by the input parameters, which distinguish only between different patient body-sizes and "fitness levels" as defined by a reference heart rate. Beyond these distinctions, the model is designed to compute the physiology for a normal Fontan patient, based on population trends, and thus will not accurately describe a patient whose physiology is drastically different from normal. Caution should be taken when applying the model to predict patient-specific responses since each Fontan patient can present a different set of cardiovascular abnormalities, which would cause the hemodynamic characteristics to deviate from the population norm in ways specific to the patient.

The two sets of clinical data used for the model development and validation only include exercise levels up to approximately 6 MET. There is no confirmation that the model will reliably estimate physiologies at higher exercise levels. The current LPN setup where the effect of the muscle pump is incorporated as a greatly reduced "effective resistance" also fundamentally limits the exercise level that can be modeled. At higher levels of exercise, either the effective resistance must become negative, or the muscle pump can no longer be approximated simply as a drop in resistance but should be modeled as an active pressure-generating source [54]. Modifications to the LPN implementation thus may be required to extend its capability to model higher exercise levels.

Perhaps most importantly, this computational model does not predict peak exercise level, which is often the target information of interest to clinicians as it directly reflects Fontan performance. Since exercise level is an input to the model, the model computes the resulting physiology under the assumption that the patient is able to exercise at the assigned level.

Being aware of these limitations, the protocol developed here can provide a highly useful tool for clinicians to estimate exercise Fontan physiologies, and for researchers to develop more advanced computational models as well as perform reductionist investigations of Fontan system interactions.

Future Work. Besides body-size and reference HR, additional input parameters that further distinguish interpatient differences could be incorporated into the model to make it more patient-specific. As additional clinical data become available, the modular framework of this protocol allows for individual exercise parameter changes to be updated accordingly, and additional exercise parameter changes to be incorporated. For example, currently, there are few clinical data available describing changes in Fontan atrial parameters with exercise. If such data were to become available, this protocol can be updated to include exercise-dependent atrial parameter changes. Retuning of the protocol will be necessary when additional exercise-dependent parameters are introduced, but the same overall framework may remain unchanged.

Further validation of the model using invasive and more extensive clinical measurements during exercise will provide additional measures of confidence in the model's ability to mimic real

physiology. Phase-contrast MRI flow and catheterization pressure measurements during exercise in a large cohort of Fontan patients will be essential for completing a more thorough validation of this exercise model. It is our hope that this work provides motivation for additional clinical data collection toward the validation and improvement of computational models of the Fontan circulation.

Summary. In this study, we developed a protocol to define model parameters for the computational simulations of a range of Fontan exercise, and performed the first direct comparison of Fontan exercise simulation results against clinical measurements. This was accomplished through analysis and synthesis of clinical and literature data, which were compiled to form a comprehensive list of physiological parameter changes during exercise. When translated into the context of a complete model of Fontan circulation, it enables the first computational model that holistically captures Fontan exercise behaviors. Two parameters from simulation results were compared against a small set of clinical data. The protocol fully defines all of the necessary simulation parameters from the patient input information, resulting in a functional model that requires no manual tuning.

The product of this work is a protocol that when given inputs of a Fontan patient body-size and reference heart rate/oxygen consumption (if available), outputs a computational model with appropriate parameters which can perform simulations of pressure and flow to describe the systemic patient physiology at various exercise levels. We have provided a complete "package" which can be adopted and used as part of a larger computational framework. For example, a multiscale setup incorporating this model may allow for investigation of Fontan venous pump operations at different exercise levels for different patient sizes, in the context of both local hemodynamics and global impacts on the systemic circulation. This protocol can also be used as a stand-alone package for investigating the interactions between different physiological parameters in the Fontan circulation and their influences on exercise physiology, which may help identify etiologies of lowered Fontan exercise capacity. The parameter changes described in this study have shown to produce physiological behaviors when interacting in a closed-loop system, thus they can provide investigators reasonable references when estimating Fontan exercise conditions. Clinical application of this protocol could allow physicians to obtain detailed quantitative reference physiologies and evaluate patients in the context of the population norm, though further validation and data are needed prior to clinical adoption. This study contributes a powerful tool to advance modeling efforts involving the exercise Fontan circulation, to allow researchers and physicians to comprehensively investigate Fontan physiology, to better identify causes of exercise intolerance, and to improve clinical management of these complex patients.

Acknowledgment

MOCHA investigators: Andrew Taylor, MD, Alessandro Giardini, MD, Sachin Khambadkone, MD, Silvia Schievano, PhD, Marc de Leval, MD, and T.-Y. Hsia, MD (Institute of Cardiovascular Sciences, UCL, London, UK); Edward Bove, MD and Adam Dorfman, MD (University of Michigan, Ann Arbor, MI, USA); G. Hamilton Baker, MD and Anthony Hlavacek (Medical University of South Carolina, Charleston, SC, USA); Francesco Migliavacca, PhD, Giancarlo Pennati, PhD, and Gabriele Dubini, PhD (Politecnico di Milano, Milan, Italy); Alison Marsden, PhD (University of California, San Diego, CA, USA); Jeffrey Feinstein, MD (Stanford University, Stanford, CA, USA); Irene Vignon-Clementel (INRIA, Paris, France); Richard Figliola, PhD and John McGregor, PhD (Clemson University, Clemson, SC, USA).

We also acknowledge Mahdi Esmaily for the Runge–Kutta code used in the model simulations. This work was supported by the Leducq Foundation as part of the Transatlantic Network of Excellence for Cardiovascular Research, a Burroughs Wellcome Fund Career award at the Scientific Interface, and an American Heart Association Postdoctoral Fellowship.

Nomenclature

In this paper, unless otherwise specified, all units of pressure, volume, flow, time, weight, and resistance are in mm Hg, ml, ml/s, s, kg, and mm Hg s ml^{-1}, respectively. Pressure references mentioned in the paper are as labeled in Fig. 1.

- BSA = body surface area in m^2
- CO = cardiac output in l/min
- EF = ejection fraction
- EDV, ESV = end diastolic and systolic volume
- HR = heart rate in beats per minute
- LPN = lumped-parameter network
- MET = metabolic equivalent in units of 3.5 ml-O_2 kg^{-1} min^{-1}
- O_2 extrac. = liter O_2 extracted per liter blood delivered (O_2 consumption/CO)
- Q_{svc}, Q_{ivc}, Q_{av}, Q_{ao} = flow through the SVC, IVC, atrioventricular valve, and aortic valve
- S_{init} = scaling factor of the initial pressures and volumes in Table 2
- SV = stroke volume
- SVC, IVC = superior and inferior vena cava
- t_{svs}, t_c = systolic and cardiac time period
- TVR, SVR, PVR = total, systemic, and pulmonary vascular resistance
- V_{sv}, V_{sa}, V_{svo}, V_{sao} = ventricular and atrial volume and reference volume

Appendix A

The LPN consists of several major blocks describing the atrium, ventricle, upper body, lower body, and pulmonary circuits. The lower-body block consists of circuits describing the major blood vessels (aorta and IVC), abdominal organs (liver, kidneys, and intestine), and legs. The heart blocks and the intrathoracic pressure (P_{ith}) generate active pressure sources for the system, where the rest of the circuit is made up of passive elements, including resistances, capacitances, inductances, and diodes, which model the viscous vascular resistance to flow, compliance of blood vessels, momentum of flowing blood, and venous valves, respectively. Each capacitance and inductance element is governed by a differential equation

$$\mathrm{Q} = \mathrm{C}\frac{\mathrm{d}\Delta\mathrm{P}}{\mathrm{dt}}$$

$$\Delta\mathrm{P} = \mathrm{L}\frac{\mathrm{dQ}}{\mathrm{dt}}$$

where C, L, ΔP, Q are the capacitance value, inductance value, pressure drop across the element, and flow into the element, respectively.

We implemented a time-varying elastance approach [55] using a ratio between the transmyocardial ventricular pressure and ventricular volume (i.e., elastance) which varies over the cardiac cycle to model the ventricular contraction. The elastance conceptually describes the "stiffness" of the ventricular chamber at any point in time as the chamber contracts and relaxes. Senzaki et al. found that the shape of the normalized (with respect to amplitude and timing of the peak) elastance waveform is relatively constant and independent of ventricular load, contractile state, and a range of cardiac diseases [55,56]. For the LPN model, we constructed a normalized elastance waveform based on the data from Senzaki et al. with smoothing applied to the diastolic part of the waveform to remove any ripples that were likely due to low signal-to-noise ratio in the experimental measurements. The waveform is zeroed

according to the value at the onset of systole and normalized to its peak, which is a similar approach that has been utilized in previous ventricular model implementation [57]. The equation below describes the mathematical construction of the normalized elastance function, using the kth coefficients "Cr" and "Ci" listed in the following table:

$$\mathrm{En(t)} = \sum_{\mathrm{k=0}}^{19} \{\mathrm{C_{rk}}\cos(2\pi\mathrm{kt}) - \mathrm{C_{ik}}\sin(2\pi\mathrm{kt})\}$$

Index K	Cr	Ci
0	2.2379×10^{-01}	$0.0000 \times 10^{+00}$
1	4.1054×10^{-02}	-4.0948×10^{-01}
2	-2.3140×10^{-01}	-2.6814×10^{-02}
3	1.7515×10^{-02}	8.5190×10^{-02}
4	1.3159×10^{-02}	-5.0110×10^{-02}
5	-4.7293×10^{-02}	2.1048×10^{-04}
6	-1.3394×10^{-03}	2.2155×10^{-02}
7	-3.9917×10^{-05}	-5.9333×10^{-03}
8	-1.2594×10^{-02}	2.4557×10^{-03}
9	-1.1214×10^{-03}	9.1653×10^{-03}
10	1.6008×10^{-03}	5.5933×10^{-04}
11	-2.9655×10^{-03}	1.6101×10^{-03}
12	4.4509×10^{-04}	3.4309×10^{-03}
13	9.5826×10^{-04}	4.0949×10^{-04}
14	4.1644×10^{-06}	5.5756×10^{-04}
15	4.1503×10^{-05}	2.1745×10^{-04}
16	-1.4608×10^{-05}	3.3081×10^{-04}
17	-9.4191×10^{-05}	1.7029×10^{-04}
18	-3.5561×10^{-05}	1.9828×10^{-04}
19	-1.3225×10^{-04}	1.4701×10^{-04}

Un-normalizing the waveform returns a simulation-specific elastance curve

$$\mathrm{E(t)} = \begin{cases} \mathrm{E_{max}En}\left(\frac{0.3}{\mathrm{t_{svs}}}\mathrm{t}\right) + \mathrm{E_{offset}}, & \frac{\mathrm{t}}{\mathrm{t_{svs}}} \le 3.33 \\ \mathrm{E_{offset}}, & \textit{elsewhere} \end{cases}$$

where En(t) and $E(t)$ are the normalized and un-normalized time-varying elastance, $E_{\max}$ and E_{offset} are constants reflecting measures of contractility and ventricular filling, respectively, and t_{svs} is the length of the systolic time period. Note that $0 \le t < t_c$, where t_c is the cardiac period.

The transmyocardial ventricular pressure is then given by

$$P_{\mathrm{tsv}}(V_{\mathrm{sv}}, \mathrm{t}) = E(\mathrm{t})(V_{\mathrm{sv}} - V_{\mathrm{svo}})$$

where V_{sv} and V_{svo} are the ventricular volume and reference volume, respectively.

The atrial behavior is modeled using a combination of a passive pressure–volume relation, an active pressure–volume relation, and an activation function [14,58,59]. The passive behavior describes the passive compliance of the atrial wall and how it responds to filling; the active behavior captures the effect of the Frank-Starling mechanism; and the activation function simulates atrial wall depolarization which determines the contribution of the active behavior to the overall atrial pressure. The atrial activation function is a construction of piecewise cosine functions as shown in Fig. 6(*a*), and described by the equation [15,17]

$$AA(t) = \begin{cases} \frac{1}{2}\left[1 - \cos\left(2\pi\dfrac{\mathrm{t} - \mathrm{t_1} + t_{\mathrm{sas}}}{t_{\mathrm{sas}}}\right)\right], & \mathrm{t} \le \mathrm{t_1} \\ \frac{1}{2}\left[1 - \cos\left(2\pi\dfrac{\mathrm{t} - t_{\mathrm{sad}} - \mathrm{t_1}}{t_{\mathrm{sas}}}\right)\right], & \mathrm{t_1} + t_{\mathrm{sad}} \le \mathrm{t} < t_c \\ 0, & \text{elsewhere} \end{cases}$$

where $t_1 = 0.2\, t_c$ and $t_{\mathrm{sas}} = 0.9\, t_{\mathrm{svs}}$.

The active and passive pressure–volume relations are described by the equations

$$P_{\mathrm{sa,active}} = \frac{V_{\mathrm{sa}} - V_{\mathrm{sao}}}{C_{\mathrm{sa}}}$$

$$P_{\mathrm{sa,active}} = P_{\mathrm{sar}}\left\{e^{D\mathrm{sa}(V_{\mathrm{sa}} - V_{\mathrm{sao}})} - 1\right\}$$

where V_{sa} and V_{sao} are the atrial volume and reference volume, respectively. C_{sa}, P_{sar}, and D_{sa} are constants which reflect atrial wall and contractile properties.

The transmyocardial atrial pressure is then given by

$$P_{\mathrm{tsa}}(V_{\mathrm{sa}}, t) = P_{\mathrm{sa,active}}\mathrm{AA}(t) + P_{\mathrm{sa,passive}}$$

Blood flow through the atrial-ventricular and aortic valves is described by the following equations [60]:

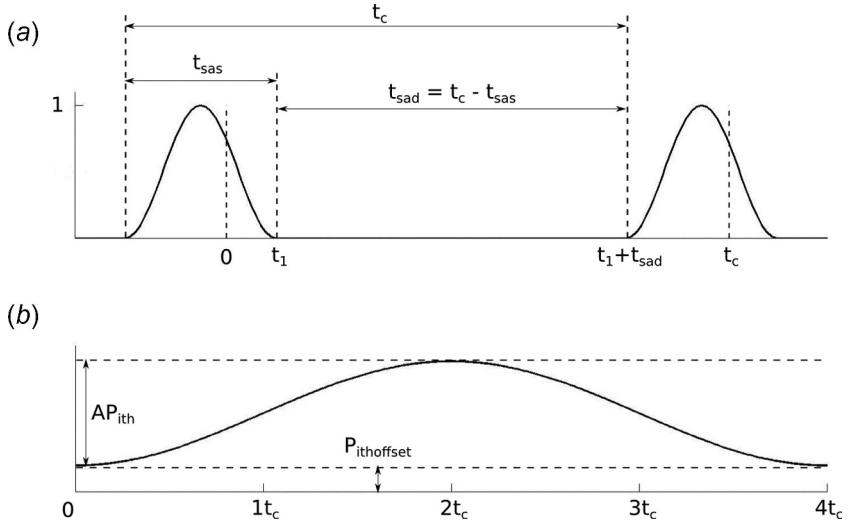

Fig. 6 (*a*) Atrial activation function and (*b*) intrathoracic pressure waveform. Note that values of AP_{ith} and $P_{\mathrm{ithoffset}}$ are typically negative during natural, nonmechanically ventilated breathing.

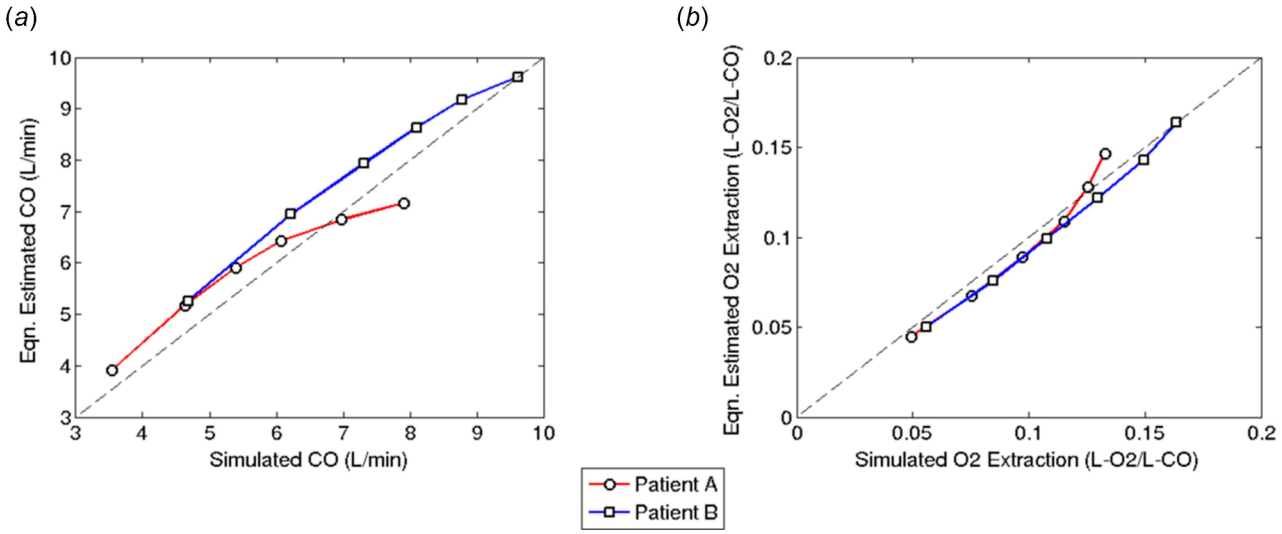

Fig. 7 Comparison of (*a*) CO and (*b*) O_2 extraction between simulation and Appendix B equation estimation for the two example patients at six MET levels

$$\frac{dQ_{av}}{dt} = \begin{cases} 0, & P_{sa} < P_{sv} \text{ and } Q_{av} \le 0 \\ \dfrac{P_{sa} - P_{sv} - K_{av}Q_{av}^2}{L_{av}}, & \text{elsewhere} \end{cases}$$

$$Q_{ao} = \begin{cases} 0, & P_{sv} < P_{ao} \\ \dfrac{1}{2K_{ao}}\sqrt{4K_{ao}(P_{sv} - P_{ao})}, & P_{sv} \ge P_{ao} \end{cases}$$

where the terms in these equations are defined in the glossary, Fig. 1, and the tables below.

We approximate the time-varying intrathoracic pressure due to breathing using a piecewise cosine waveform as shown in Fig. 6(*b*). The intrathoracic pressure acts as an extravascular pressure to the large blood vessels in the thorax, the pulmonary vasculature, and the heart, and thus is connected to the corresponding elements in the LPN. Relative to the intrathoracic pressure, the intra-abdominal pressure does not have significant effects on blood flow, and thus is not included in the model.

The following tables provide the constant parameter values in the LPN:

Inductance (mm Hg s^2 ml^{-1})	
L_{av}	1.00×10^{-05}
L_{tha}	1.33×10^{-03}
L_{aba}	1.33×10^{-03}
L_{lega}	1.33×10^{-03}
L_{uba}	5.48×10^{-04}
Heart parameter	
C_{sa} (ml mm Hg^{-1})	0.75
P_{sar} (mm Hg)	0.35
D_{sa} (ml^{-1})	0.225
V_{sao} (ml)	15
K_{av} (mm Hg s^2 ml^{-2})	2.3×10^{-05}
K_{ao} (mm Hg s^2 ml^{-2})	1.15×10^{-05}

Finally, the functions described in this section, together with the system of algebraic and ordinary differential equations derived from the LPN, were solved using a fourth order Runge–Kutta method.

Appendix B

The correlations between exercise level MET and cardiac index and O_2 extraction, found in the clinical data collected in nine Fontan patients at rest and during different levels of exercise

$$\text{Cardiac index} = 1.2578\ \ln(\text{MET}) + 2.7136\ \ (R^2 = 0.7175)$$

$$O_2\ \text{extrac.} = 0.0197\ \text{MET} + 0.0295\ \ (R^2 = 0.8122)$$

Applying these equations to estimate CO and O_2 extraction in example patients A and B each at six different MET levels, Fig. 7 shows the comparison of the equation estimation with corresponding model simulation results.

References

[1] Marino, B., 2002, "Outcomes after the Fontan Procedure," Curr. Opin. Pediatr., **14**(5), pp. 620–626.

[2] Gewillig, M. H., Lundström, U. R., Bull, C., Wyse, R. K., and Deanfield, J. E., 1990, "Exercise Responses in Patients With Congenital Heart Disease After Fontan Repair: Patterns and Determinants of Performance," J. Am. Coll. Cardiol., **15**(6), pp. 1424–1432.

[3] Durongpisitkul, K., Driscoll, D. J., Mahoney, D. W., Wollan, P. C., Mottram, C. D., Puga, F. J., and Danielson, G. K., 1997, "Cardiorespiratory Response to Exercise After Modified Fontan Operation: Determinants of Performance," J. Am. Coll. Cardiol., **29**(4), pp. 785–790.

[4] Yang, W., Vignon-Clementel, I. E., Troianowski, G., Reddy, V. M., Feinstein, J. A., and Marsden, A. L., 2011, "Hepatic Blood Flow Distribution and Performance in Conventional and Novel Y-Graft Fontan Geometries: A Case Series Computational Fluid Dynamics Study," J. Thorac. Cardiovasc. Surg., **143**, pp. 1086–1097.

[5] Whitehead, K. K., Pekkan, K., Kitajima, H. D., Paridon, S. M., Yoganathan, A. P., and Fogel, M. A., 2007, "Nonlinear Power Loss During Exercise in Single-Ventricle Patients After the Fontan: Insights From Computational Fluid Dynamics," Circulation, **116**(11 Suppl), pp. I165–I171.

[6] Justino, H., Benson, L., and Freedom, R., 2001, "Development of Unilateral Pulmonary Arteriovenous Malformations Due to Unequal Distribution of Hepatic Venous Flow," Circulation, **103**(8), pp. E39–E40.

[7] Srivastava, D., Preminger, T., Lock, J. E., Mandell, V., Keane, J. F., Mayer, J. E., Kozakewich, H., and Spevak, P. J., 1995, "Hepatic Venous Blood and the Development of Pulmonary Arteriovenous Malformations in Congenital Heart Disease," Circulation, **92**(5), pp. 1217–1222.

[8] Shachar, G. B., Fuhrman, B. P., Wang, Y., Lucas, R. V., and Lock, J. E., 1982, "Rest and Exercise Hemodynamics After the Fontan Procedure," Circulation, **65**(6), pp. 1043–1048.

[9] Goldstein, B. H., Connor, C. E., Gooding, L., and Rocchini, A. P., 2010, "Relation of Systemic Venous Return, Pulmonary Vascular Resistance, and Diastolic Dysfunction to Exercise Capacity in Patients With Single Ventricle Receiving Fontan Palliation," Am. J. Cardiol., **105**(8), pp. 1169–1175.

[10] Migliavacca, F., Balossino, R., Pennati, G., Dubini, G., Hsia, T. Y., De Leval, M. R., and Bove, E. L., 2006, "Multiscale Modelling in Biofluidynamics: Application to Reconstructive Paediatric Cardiac Surgery," J. Biomech., **39**(6), pp. 1010–1020.

[11] Taylor, C. A., Draney, M. T., Ku, J. P., Parker, D., Steele, B. N., Wang, K., and Zarins, C. K., 1999, "Predictive Medicine: Computational Techniques in Therapeutic Decision-Making," Comput. Aided Surg., **4**(5), pp. 231–247.
[12] Degroff, C. G., 2008, "Modeling the Fontan Circulation: Where We Are and Where We Need to Go," Pediatr. Cardiol., **29**(1), pp. 3–12.
[13] Marsden, A. L., Vignon-Clementel, I. E., Chan, F. P., Feinstein, J. A., and Taylor, C. A., 2007, "Effects of Exercise and Respiration on Hemodynamic Efficiency in Cfd Simulations of the Total Cavopulmonary Connection," Ann. Biomed. Eng., **35**(2), pp. 250–263.
[14] Baretta, A., Corsini, C., Marsden, A. L., Vignon-Clementel, I. E., Hsia, T. Y., Dubini, G., Migliavacca, F., and Pennati, G., 2012, "Respiratory Effects on Hemodynamics in Patient-Specific CFD Models of the Fontan Circulation Under Exercise Conditions," Eur. J. Mech. B, **35**, pp. 61–69.
[15] Snyder, M. F., and Rideout, V. C., 1969, "Computer Simulation Studies of the Venous Circulation," IEEE Trans. Biomed Eng., **16**(4), pp. 325–334.
[16] Kung, E., Baretta, A., Baker, C., Arbia, G., Biglino, G., Corsini, C., Schievano, S., Vignon-Clementel, I. E., Dubini, G., and Pennati, G., 2012, "Predictive Modeling of the Virtual Hemi-Fontan Operation for Second Stage Single Ventricle Palliation: Two Patient-Specific Cases," J. Biomech., **46**, pp. 423–429.
[17] Migliavacca, F., Pennati, G., Dubini, G., Fumero, R., Pietrabissa, R., Urcelay, G., Bove, E., Hsia, T., and De Leval, M., 2001, "Modeling of the Norwood Circulation: Effects of Shunt Size, Vascular Resistances, and Heart Rate," Am. J. Physiol. Heart Circ. Physiol., **280**(5), pp. H2076–H2086. Available at: http://ajpheart.physiology.org/content/280/5/H2076
[18] Corsini, C., Baker, C., Kung, E., Schievano, S., Arbia, G., Baretta, A., Biglino, G., Migliavacca, F., Dubini, G., and Pennati, G., 2013, "An Integrated Approach to Patient-Specific Predictive Modeling for Single Ventricle Heart Palliation," Comput. Methods Biomech. Biomed. Eng, (in press).
[19] Giardini, A., Balducci, A., Specchia, S., Gargiulo, G., Bonvicini, M., and Picchio, F., 2008, "Effect of Sildenafil on Haemodynamic Response to Exercise and Exercise Capacity in Fontan Patients," Eur. Heart J., **29**(13), pp. 1681–1687.
[20] Gabrielsen, A., Videbaek, R., Schou, M., Damgaard, M., Kastrup, J., and Norsk, P., 2002, "Non-Invasive Measurement of Cardiac Output in Heart Failure Patients Using a New Foreign Gas Rebreathing Technique," Clin. Sci., **102**(2), pp. 247–252.
[21] Sheth, S. S., Maxey, D. M., Drain, A. E., and Feinstein, J. A., 2012, "Validation of the Innocor Device for Noninvasive Measurement of Oxygen Consumption in Children and Adults," Pediatr. Cardiol., **34**, pp. 847–852.
[22] West, G. B., and Brown, J. H., 2005, "The Origin of Allometric Scaling Laws in Biology From Genomes to Ecosystems: Towards a Quantitative Unifying Theory of Biological Structure and Organization," J. Exp. Biol., **208**(Pt 9), pp. 1575–1592.
[23] Dewey, F. E., Rosenthal, D., Murphy, D. J., Froelicher, V. F., and Ashley, E. A., 2008, "Does Size Matter? Clinical Applications of Scaling Cardiac Size and Function for Body Size," Circulation, **117**(17), pp. 2279–2287.
[24] Gewillig, M., Brown, S. C., Eyskens, B., Heying, R., Ganame, J., Budts, W., La Gerche, A., and Gorenflo, M., 2010, "The Fontan Circulation: Who Controls Cardiac Output?," Interact. Cardiovasc. Thorac. Surg., **10**(3), pp. 428–433.
[25] Stickland, M. K., Welsh, R. C., Petersen, S. R., Tyberg, J. V., Anderson, W. D., Jones, R. L., Taylor, D. A., Bouffard, M., and Haykowsky, M. J., 2006, "Does Fitness Level Modulate the Cardiovascular Hemodynamic Response to Exercise?," J. Appl. Physiol., **100**(6), pp. 1895–1901.
[26] Cui, W., Roberson, D., Chen, Z., Madronero, L., and Cuneo, B., 2008, "Systolic and Diastolic Time Intervals Measured from Doppler Tissue Imaging: Normal Values and Z-Score Tables, and Effects of Age, Heart Rate, and Body Surface Area," J. Am. Soc. Echocardiogr., **21**(4), pp. 361–370.
[27] Gemignani, V., Bianchini, E., Faita, F., Giannoni, M., Pasanisi, E., Picano, E., and Bombardini, T., 2008, "Assessment of Cardiologic Systole and Diastole Duration in Exercise Stress Tests With a Transcutaneous Accelerometer Sensor," Comput. Cardiol., **35**, pp. 153–156.
[28] Mitchell, J. H., 1963, "Mechanisms of Adaptation of the Left Ventricle to Muscular Exercise," Pediatrics, **32**(4), pp. 660–670. Available at: http://pediatrics.aappublications.org/content/32/4/660.short
[29] Alpert, B. S., Benson, L., and Olley, P. M., 1981, "Peak Left Ventricular Pressure/Volume (Emax) During Exercise in Control Subjects and Children With Left-Sided Cardiac Disease," Cathet. Cardiovasc. Diagn., **7**(2), pp. 145–153.
[30] Bombardini, T., Nevola, E., Giorgetti, A., Landi, P., Picano, E., and Neglia, D., 2008, "Prognostic Value of Left-Ventricular and Peripheral Vascular Performance in Patients With Dilated Cardiomyopathy," J. Nucl. Cardiol., **15**(3), pp. 353–362.
[31] Dexter, L., Whittenberger, J. L., Haynes, F. W., Goodale, W. T., Gorlin, R., and Sawyer, C. G., 1951, "Effect of Exercise on Circulatory Dynamics of Normal Individuals," J. Appl. Physiol., **3**(8), pp. 439–453. Available at: http://journals.lww.com/ajpmr/Citation/1952/12000/Effect_of_Exercise_on_Circulatory_Dynamics_of.7.aspx
[32] Kasalický, J., Hurych, J., Widimský, J., Dejdar, R., Metys, R., and Staněk, V., 1968, "Left Heart Haemodynamics at Rest and During Exercise in Patients With Mitral Stenosis," Br. Heart J., **30**(2), pp. 188–195.
[33] Yu, P. N., Murphy, G. W., Schreiner, Jr, B. F., and James, D. H., 1967, "Distensibility Characteristics of the Human Pulmonary Vascular Bed: Study of the Pressure-Volume Response to Exercise in Patients With and Without Heart Disease," Circulation, **35**(4), pp. 710–723.
[34] Ekelund, L. G., and Holmgren, A., 1964, "Circulatory and Respiratory Adaptation, During Long-Term, Non-Steady State Exercise, in the Sitting Position," Acta Physiol. Scand., **62**(3), pp. 240–255.
[35] Holmgren, A., Jonsson, B., and Sjöstrand, T., 1960, "Circulatory Data in Normal Subjects at Rest and During Exercise in Recumbent Position, With Special Reference to the Stroke Volume at Different Work Intensities," Acta Physiol. Scand., **49**(4), pp. 343–363.
[36] Luepker, R. V., Holmberg, S., and Varnauskas, E., 1971, "Left Atrial Pressure During Exercise in Hemodynamic Normals," Am. Heart J., **81**(4), pp. 494–497.
[37] Slonim, N. B., Ravin, A., Balchum, O. J., and Dressler, S. H., 1954, "The Effect of Mild Exercise in the Supine Position on the Pulmonary Arterial Pressure of Five Normal Human Subjects," J. Clin. Invest., **33**(7), pp. 1022–1030.
[38] Barratt-Boyes, B. G., and Wood, E. H., 1957, "Hemodynamic Response of Healthy Subjects to Exercise in the Supine Position While Breathing Oxygen," J. Appl. Physiol., **11**(1), pp. 129–135. Available at: http://jap.physiology.org/content/11/1/129.short
[39] Sancetta, S. M., and Rakita, L., 1957, "Response of Pulmonary Artery Pressure and Total Pulmonary Resistance of Untrained, Convalescent Man to Prolonged Mild Steady State Exercise," J. Clin. Invest., **36**(7), pp. 1138–1149.
[40] Widimsky, J., Berglund, E., and Malmberg, R., 1963, "Effect of Repeated Exercise on the Lesser Circulation," J. Appl. Physiol., **18**(5), pp. 983–986. Available at: http://jap.physiology.org/content/18/5/983.short
[41] Wallace, A. G., Mitchell, J. H., Skinner, N. S., and Sarnoff, S. J., 1963, "Hemodynamic Variables Affecting the Relation Between Mean Left Atrial and Left Ventricular End-Diastolic Pressures," Circ. Res., **13**, pp. 261–270.
[42] Manohar, M., 1993, "Pulmonary Artery Wedge Pressure Increases With High-Intensity Exercise in Horses," Am. J. Vet. Res., **54**(1), pp. 142–146. Available at: http://www.ncbi.nlm.nih.gov/pubmed/8427458
[43] Cheng, C. P., Igarashi, Y., and Little, W. C., 1992, "Mechanism of Augmented Rate of Left Ventricular Filling During Exercise," Circ. Res., **70**(1), pp. 9–19.
[44] Nevsky, G., Jacobs, J. E., Lim, R. P., Donnino, R., Babb, J. S., and Srichai, M. B., 2011, "Sex-Specific Normalized Reference Values of Heart and Great Vessel Dimensions in Cardiac CT Angiography," AJR Am. J. Roentgenol., **196**(4), pp. 788–794.
[45] Carroll, J. D., Hess, O. M., Hirzel, H. O., and Krayenbuehl, H. P., 1983, "Dynamics of Left Ventricular Filling at Rest and During Exercise," Circulation, **68**(1), pp. 59–67.
[46] Grimby, G., Goldman, M., and Mead, J., 1976, "Respiratory Muscle Action Inferred from Rib Cage and Abdominal Vp Partitioning," J. Appl. Physiol., **41**(5), pp. 739–751. Available at: http://www.jappl.org/content/41/5/739.short
[47] Armstrong, R. B., Delp, M. D., Goljan, E. F., and Laughlin, M. H., 1987, "Distribution of Blood Flow in Muscles of Miniature Swine During Exercise," J. Appl. Physiol., **62**(3), pp. 1285–1298. Avaiable at: http://www.jappl.org/content/62/3/1285.short
[48] Pennati, G., and Fumero, R., 2000, "Scaling Approach to Study the Changes Through the Gestation of Human Fetal Cardiac and Circulatory Behaviors," Ann. Biomed. Eng., **28**, pp. 442–452.
[49] Clausen, J. P., Klausen, K., Rasmussen, B., and Trap-Jensen, J., 1973, "Central and Peripheral Circulatory Changes After Training of the Arms or Legs," Am. J. Physiol., **225**(3), pp. 675–682. Available at: http://ajplegacy.physiology.org/content/225/3/675.extract
[50] Hjortdal, V. E., Emmertsen, K., Stenbøg, E., Fründ, T., Schmidt, M. R., Kromann, O., Sørensen, K., and Pedersen, E. M., 2003, "Effects of Exercise and Respiration on Blood Flow in Total Cavopulmonary Connection: A Real-Time Magnetic Resonance Flow Study," Circulation, **108**(10), pp. 1227–1231.
[51] Marsden, A. L., Reddy, V. M., Shadden, S. C., Chan, F. P., Taylor, C. A., and Feinstein, J. A., 2010, "A New Multiparameter Approach to Computational Simulation for Fontan Assessment and Redesign," Congenit Heart Dis., **5**(2), pp. 104–117.
[52] Koeken, Y., Arts, T., and Delhaas, T., 2012, "Simulation of the Fontan Circulation During Rest and Exercise," Annual International Conference of the IEEE Engineering in Medicine and Biology Society, San Diego, CA, Aug. 28–Sept. 1, 2012, pp. 6673–6676.
[53] Sundareswaran, K. S., Pekkan, K., Dasi, L. P., Whitehead, K., Sharma, S., Kanter, K. R., Fogel, M. A., and Yoganathan, A. P., 2008, "The Total Cavopulmonary Connection Resistance: A Significant Impact on Single Ventricle Hemodynamics at Rest and Exercise," Am. J. Physiol. Heart Circ. Physiol., **295**(6), pp. H2427–H2435.
[54] Folkow, B., Gaskell, P., and Waaler, B. A., 1970, "Blood Flow through Limb Muscles During Heavy Rhythmic Exercise," Acta Physiol. Scand., **80**(1), pp. 61–72.
[55] Suga, H., Sagawa, K., and Shoukas, A. A., 1973, "Load Independence of the Instantaneous Pressure-Volume Ratio of the Canine Left Ventricle and Effects of Epinephrine and Heart Rate on the Ratio," Circulation Research, **32**(3), pp. 314–322.
[56] Senzaki, H., Chen, C., and Kass, D., 1996, "Single-Beat Estimation of End-Systolic Pressure-Volume Relation in Humans: A New Method with the Potential for Noninvasive Application," Circulation, **94**(10), pp. 2497–2506.
[57] Segers, P., Stergiopulos, N., Westerhof, N., Wouters, P., Kolh, P., and Verdonck, P., 2003, "Systemic and Pulmonary Hemodynamics Assessed With a Lumped-Parameter Heart-Arterial Interaction Model," J. Eng. Math., **47**, pp. 185–199.
[58] Avanzolini, G., Barbini, P., Cappello, A., and Cevese, A., 1985, "Time-Varying Mechanical Properties of the Left Ventricle-A Computer Simulation," Biomed. Eng. IEEE Trans., **10**, pp. 756–763.
[59] Lau, V.-K., and Sagawa, K., 1979, "Model Analysis of the Contribution of Atrial Contraction to Ventricular Filling," Ann. Biomed. Eng., **7**(2), pp. 167–201.
[60] Peskin, C. S., 1982, "The Fluid Dynamics of Heart Valves: Experimental, Theoretical, and Computational Methods," Ann. Rev. Fluid Mech., **14**(1), pp. 235–259.